Numerical investigation of three-dimensional single-species plasma equilibria on magnetic surfaces

Remi G. Lefrancois, Thomas Sunn Pedersen, Allen H. Boozer, and Jason P. Kremer
Department of Applied Physics and Applied Mathematics, Columbia University, New York, New York 10027

(Received 17 December 2004; accepted 11 April 2005; published online 23 June 2005)

Presented for the first time are numerical solutions to the three-dimensional nonlinear equilibrium equation for single-species plasmas confined on magnetic surfaces and surrounded by an equipotential boundary. The major-radial shift of such plasmas is found to be outward, qualitatively similar to the Shafranov shift of quasineutral plasmas confined on magnetic surfaces. However, this is the opposite of what occurs in the pure toroidal field equilibria of non-neutral plasmas (i.e., in the absence of magnetic surfaces). The effect of varying the number of Debye lengths in the plasma for the three-dimensional (3D) model is in agreement with previous 2D calculations: the potential varies significantly on magnetic surfaces for plasmas with few Debye lengths ($a \lesssim \lambda_d$), and tends to be constant on surfaces when many Debye lengths are present ($a \gtrsim 10\lambda_d$). For the case of a conducting boundary that does not conform to the outer magnetic surface, the plasma is shifted towards the conductor and the potential varies significantly on magnetic surfaces near the plasma edge. Debye shielding effects are clearly demonstrated when a nonuniform bias is applied to the boundary. Computed equilibrium profiles are presented for the Columbia Non-Neutral Torus [T. S. Pedersen, A. H. Boozer, J. P. Kermer, R. Lefrancois, F. Dahlgren, N. Pomphrey, W. Reiersen, and W. Dorland, Fusion Sci. Technol. **46**, 200 (2004)], a stellarator designed to confine non-neutral plasmas. © *2005 American Institute of Physics*. [DOI: 10.1063/1.1928248]

I. INTRODUCTION

The confinement of non-neutral plasmas on magnetic surfaces is a relatively new area of study. This may be due to the generally complex and expensive devices required to produce magnetic surfaces (stellarators and tokamaks), and to the great success of Penning traps at confining single-species plasmas. Using a remarkably simple coil set (four circular coils) to generate magnetic surfaces, the Columbia Non-neutral Torus (CNT) is the first stellarator designed specifically to study the confinement of non-neutral and partially neutralized plasmas.[1]

While Penning traps are limited to the confinement of like-charged particles, a magnetic surface configuration such as that of a stellarator can confine plasmas of arbitrary neutrality.[2]

This type of device is capable of exploring a wide range of new physical phenomena with relevance to basic plasma physics, particle physics, and fusion science. By introducing positrons into an electron plasma confined on magnetic surfaces, a plasma can be formed in which positrons are confined not only by the magnetic surfaces, but also by the potential well created by the electrons.[3] Injecting antiprotons into a positron plasma may be a way of producing large quantities of neutral antimatter, providing an opportunity for detailed measurements of the energy levels of antihydrogen. A partially neutralized plasma generates large electric fields; the effects of such fields on plasma confinement in a stellarator have not yet been studied.

The first physics goal of the CNT, which has recently come online, will be the confinement of pure electron plasmas on magnetic surfaces. A direct comparison between the actual experimental equilibria and those calculated from theory requires a numerical algorithm in three dimensions that can properly incorporate realistic boundary conditions on the electric potential. In this paper we describe the implementation of such an algorithm and discuss computational results for a variety of magnetic surface and boundary configurations, including those of the CNT.

II. THEORY

The equilibrium of a low density ($n \ll n_B = \epsilon_0 B^2/2m_e$ (Ref. 4) and $n \ll \epsilon_0 Bc/ae$) electron plasma confined on magnetic surfaces is described by the Poisson–Boltzmann equation for the electrostatic potential Φ (Ref. 5),

$$\nabla^2 \Phi = \frac{e}{\epsilon_0} N(\psi) \exp\left(\frac{e\Phi}{T_e(\psi)}\right), \tag{1}$$

where ψ is the magnetic surface coordinate (ϕ and θ will be used throughout this paper as the toroidal and poloidal angles, respectively). We have the freedom to prescribe $N(\psi)$, which, along with the exponential term, determines the density. The two upper limits on density given above ensure, respectively, that the convective term in the force balance is negligible and that plasma currents will not alter the externally imposed magnetic field.

We express the temperature as $T_e(\psi) = T_0 \alpha(\psi)$, where $\alpha(0) = 1$. Except where noted, results presented in this paper are for flat temperature profiles, $\alpha(\psi) = 1$. We expect a roughly uniform temperature due to rapid cross-surface heat transport.[6]

The equilibrium equation is given by Poisson's equation combined with a parallel balance between the electrostatic force and the pressure gradient (in other words, a force balance along each magnetic field line). Each field line maps out a magnetic surface, a surface over which the field line comes arbitrarily close to every point. A pure toroidal field, which does not possess magnetic surfaces, exhibits very different equilibria[7] from those of Eq. (1).

Equation (1) can be nondimensionalized[8] as

$$\tilde{\nabla}^2\tilde{\Phi} = s(\psi)\exp[\tilde{\Phi}/\alpha(\psi)] = \tilde{n}, \tag{2}$$

where $\tilde{\Phi}=e\Phi/T_0$, $s(\psi)=N(\psi)/N(0)$, $\tilde{x}=x/s_D$, $s_D=\sqrt{\epsilon_0 T_0/N(0)e^2}$, and $\tilde{n}$ is a dimensionless density. The size of the plasma is measured in units of the characteristic scale length s_D which we relate to the Debye length ($\lambda_d=\sqrt{\epsilon_0 T_e/ne^2}$) at $\psi=0$, $\phi=0$,

$$s_D = \lambda_D(\psi=0,\phi=0)\exp\left[-\frac{\tilde{\Phi}(\psi=0,\phi=0)}{2}\right]. \tag{3}$$

The length s_D is the only adjustable scale in the dimensionless problem, and provides a relation between the temperature, density, and size of the plasma. The computational domain is specified initially in units of s_D, and converted to units of $\lambda_D(\psi=0,\phi=0)$ once the solution for $\tilde{\Phi}$ is known. Physical quantities can then be obtained from the definition of the Debye length by specifying two of the following in physical units: density (at any point in the plasma), temperature, and plasma size.

By varying the size of the domain, we can create plasmas that are large/cold/dense or small/hot/rare. As the number of Debye lengths in the plasma goes to zero, T_e becomes much larger than $|e\Phi|$, so the exponential term in the equilibrium equation approaches unity. The equilibrium is then given simply by Poisson's equation where $N(\psi)$ is the density. In this case, the pressure gradient dominates over the electrostatic force and the plasma spreads itself evenly over each field line (and therefore each magnetic surface). The potential is simply a function of the boundary conditions and the fixed density profile, and can vary significantly on a magnetic surface. As the number of Debye lengths in the plasma goes to infinity, the electrostatic force dominates, so the potential must be nearly constant on a magnetic surface to maintain force balance, while the density can vary significantly. These limits have been confirmed for two-dimensional solutions of the equilibrium equation.[8]

III. COMPUTATIONAL METHOD

A. Iterative process

For a single-species plasma, $a \gg \lambda_D$ implies $|e\Phi/T_e| \gg 1$, so the equilibrium equation cannot be linearized. Instead, a pseudospectral Fourier method is used for the calculation of three-dimensional (3D) equilibria (identical to that used previously for 2D calculations[8]). This is an iterative Fourier method in which the nonlinear term is evaluated in real space.

Denoting the right-hand side of Eq. (2) as $f=s(\psi)\exp[\tilde{\Phi}/\alpha(\psi)]$, and assigning to Fourier components the superscript **k** (wave number), the equilibrium equation is

$$0 = -f^{\mathbf{k}} - k^2\tilde{\Phi}^{\mathbf{k}}. \tag{4}$$

We add a term that provides a smooth path from some nonequilibrium $\tilde{\Phi}^{\mathbf{k}}$ to the equilibrium solution,

$$\frac{\partial\tilde{\Phi}^{\mathbf{k}}}{\partial t} = -f^{\mathbf{k}} - k^2\tilde{\Phi}^{\mathbf{k}}, \tag{5}$$

then set $\partial\tilde{\Phi}^{\mathbf{k}} \to \tilde{\Phi}^{\mathbf{k}}_j - \tilde{\Phi}^{\mathbf{k}}_{j-1}$, $\partial t \to \delta t$ (the step size), and $f^{\mathbf{k}} \to f^{\mathbf{k}}_{j-1}$, where j is the iteration number, to obtain an iterative equation for $\tilde{\Phi}^{\mathbf{k}}_j$,

$$\tilde{\Phi}^{\mathbf{k}}_j = \frac{\tilde{\Phi}^{\mathbf{k}}_{j-1} - \delta t f^{\mathbf{k}}_{j-1}}{1 + k^2\delta t}. \tag{6}$$

We start the process by specifying an initial guess for $\tilde{\Phi}_0$ (typically zero everywhere), from which f_0 is obtained. The Fourier transform is then taken ($f^{\mathbf{k}}_0$), and $\tilde{\Phi}^{\mathbf{k}}_1$ is obtained from Eq. (6). This process is repeated until the equilibrium equation is satisfied to within an average error of 10^{-6}, where the error field is defined as the difference between the two sides of Eq. (2) divided by the average of the left-hand side.

As an added complication, the relation between $s(\psi)$ and $\tilde{n}$ is not known *a priori* since $\tilde{\Phi}$ is not known. We therefore choose to update $s(\psi)$ during the iterative process in order to have some control over the density profile. For this paper, we enforce a parabolic density at $\phi=\pi/2$, $\theta=0$,

$$\frac{\tilde{n}(r,\pi/2,0)}{\tilde{n}(\psi=0,\phi=\pi/2)} = 1 - \frac{r^2}{a^2}, \tag{7}$$

where r is the minor radial coordinate and a is the minor radius (or more generally, the minor radial coordinate of the plasma boundary at $\phi=\pi/2$, $\theta=0$). We evaluate the $s[\psi(r,\pi/2,0)]$ required to generate this density using Eq. (2),

$$s[\psi(r,\pi/2,0)] = \left(1 - \frac{r^2}{a^2}\right) \times \exp\left[\frac{-\tilde{\Phi}(r,\pi/2,0)}{\alpha(\psi)} + \tilde{\Phi}(\psi=0,\phi=\pi/2)\right]. \tag{8}$$

Using a spline routine, $s(\psi)$ is obtained for all other grid points.

For all computational results presented, convergence was obtained in roughly 10^4 iterations for plasmas with many Debye lengths ($a \approx 10\lambda_d$). Convergence is much more rapid for plasmas with fewer Debye lengths ($a \approx \lambda_d$), $\approx 10^3$ iterations. This is roughly the same as for 2D equilibria and is independent of grid size. A 64^3 grid was used for all equilibrium calculations except for those of the CNT, which required a 128^3 grid due to the more complicated geometry. This code was implemented entirely in Interactive Data Language (IDL).

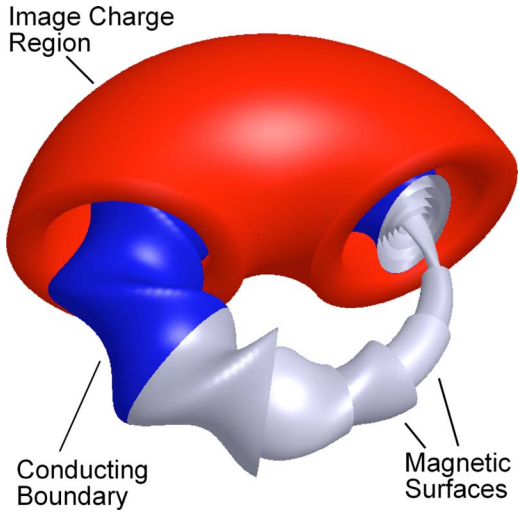

FIG. 1. (Color online). Cutaway view of an image charge region, conducting boundary, and magnetic surfaces.

B. Boundary conditions

An image charge distribution is used to maintain a constant potential on the conducting boundary (Fig. 1). The required density profile of the image charge is calculated at each iteration using a singular value decomposition (SVD) method.

The image charge modes have the form

$$\tilde{n}_{lm} = A_{lm} g(r) \exp(il\theta) \exp(im\phi), \tag{9}$$

where $g(r)=1+\sin(\gamma r+\delta)$ inside the image charge region and $g(r)=0$ outside. The constants γ and δ are chosen such that $g(r)$ goes through one full period in the image charge region, with zeros at the edges. This provides a smooth distribution with a well-behaved Fourier transform.

The ϕ and θ Fourier modes of the potential on the conducting boundary due to the image charge can be expressed in matrix form as

$$\tilde{\Phi}_n = D_{np} A_p, \tag{10}$$

where n is an index that runs through all combinations of ϕ and θ Fourier modes (of the potential on the boundary), p is the index of the image charge mode (l,m) from Eq. (2), and A_p is the magnitude of the p^{th} image charge mode.

Before starting the iterative process, we determine the coupling matrix D_{np}. To obtain the p^{th} column of D_{np}, the image charge associated with unity amplitude of the p^{th} charge mode is applied to the grid, and a Fourier method is used to solve for the potential everywhere $(\tilde{\Phi}^{\mathbf{k}}=\tilde{\rho}^{\mathbf{k}}/k^2)$. Since we are dividing by k^2, the zeroth density mode must be zero. A spherical shell of charge, which adds only a constant term to the boundary, is used to balance the net image charge. Once the potential is calculated everywhere, it is interpolated onto the boundary, and the resulting Fourier components form the p^{th} column of D_{np}.

Standard SVD inversion routines are then used to obtain D^{+}_{pn}, the pseudoinverse of D_{np}. The magnitudes of the image charge modes required to produce some given potential $\tilde{\Phi}_n$ on the boundary are

$$A_p = D^{+}_{pn} \tilde{\Phi}_n. \tag{11}$$

At each iteration the vector $\tilde{\Phi}_n$ is calculated and the charge required to produce it [from Eq. (11)] is subtracted from the grid, canceling the variation in potential on the conducting boundary. The combination of image charge modes that produces a constant potential on the boundary is then added in the appropriate amount to maintain overall charge neutrality.

IV. RESULTS

A. Toroidally symmetric surfaces

1. Conforming boundary

The simplest three-dimensional solutions to the equilibrium equation involve toroidally symmetric magnetic surfaces with circular cross section and conforming equipotential boundary. These equilibria demonstrate the major-radial density shift, as well as the effect of varying the number of Debye lengths in the plasma. The plasmas discussed in this section, and throughout this paper, have aspect ratios of $R/a \approx 2$.

Contours of constants Φ, n, and ψ for a plasma with many Debye lengths ($a \approx 10\lambda_d$) are shown in the top plot of Fig. 2. If this were an $a=0.1$ m plasma with a peak density of 10^{12} m^{-3}, the temperature would be roughly 0.75 eV and the potential on the magnetic axis would be -30 V with respect to the conducting boundary. The minimum magnetic field required to confine such a plasma (based on density limits) is around 10^{-3} T.

The Φ and ψ contours are nearly identical, while the density contours are shifted outward, away from the centerline. This outward shift of density is the opposite of what is observed for pure toroidal field equilibria,[9] where the plasma contracts.[10,11]

In the case of a pure toroidal field, there is a bulk force balance between the attraction of the plasma to the inner conducting wall and the hoop force pushing the plasma outward.

When rigid magnetic surfaces are present, the force balance occurs *along a field line*, where the hoop force causes the density to build up on the outer part of the surface. The hoop force in this case is driven by electrostatic repulsion, and it is a combination of electrostatic self-repulsion and pressure that provides the restoring force, pushing the plasma back toward the inboard side of the surface.

The effect is qualitatively similar to the Shafranov shift of a quasineutral plasma confined on magnetic surfaces, but the underlying physics in the latter case is very different and involves a shift of magnetic surfaces.

A plasma containing fewer Debye lengths ($a \approx \lambda_d$) is shown in the bottom plot of Fig. 2. If this were an $a=0.1$ m plasma with a peak density of 10^{12} m^{-3}, the tempera-

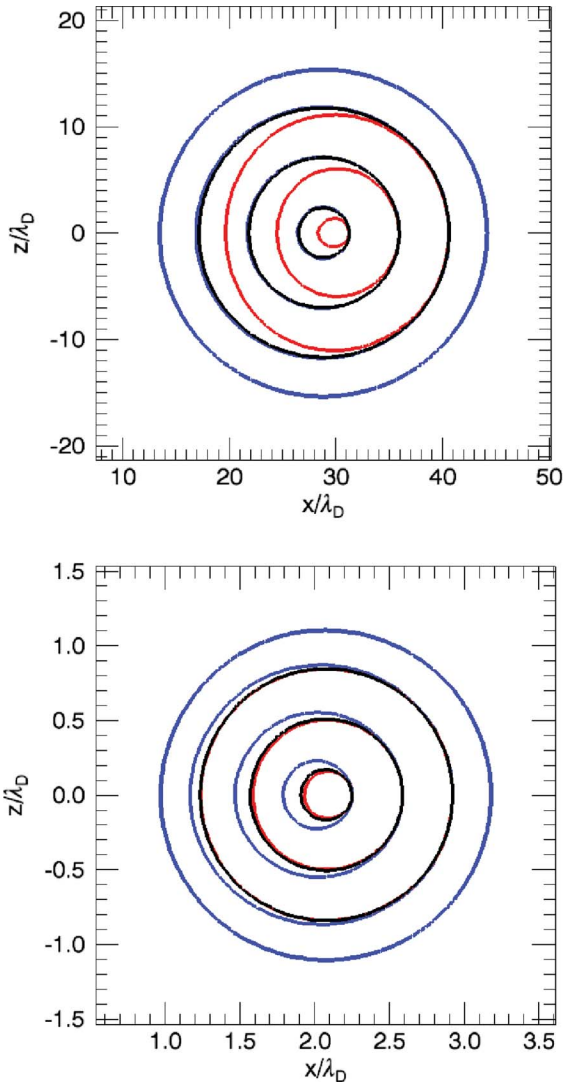

FIG. 2. (Color). Toroidally symmetric surfaces. Many Debye lengths (top), few Debye lengths (bottom). Contours of constant Φ (blue), n (red), and ψ (black). The centerline is to the left at $x/\lambda_D=0$.

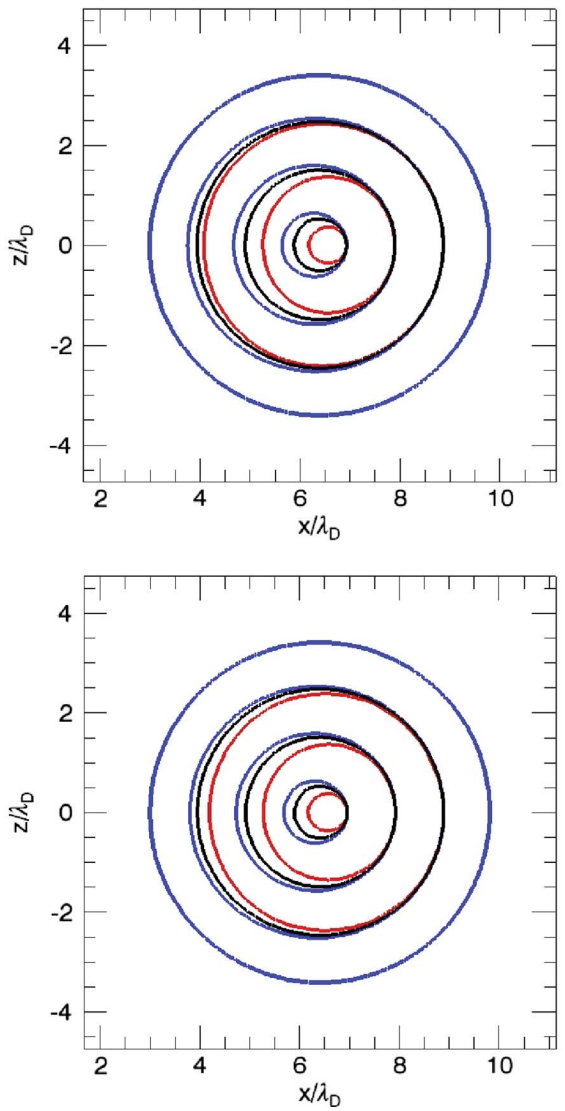

FIG. 3. (Color). Temperature profiles. Constant temperature (top), parabolic temperature (bottom). Contours of constant Φ (blue), n (red), and ψ (black) for an $a/\lambda_D \approx 3$ plasma.

ture would be roughly 150 eV and the potential on axis −30 V with respect to the conducting boundary.

Due to its higher pressure, the plasma is able to spread out uniformly over a magnetic surface, causing n and ψ contours to nearly coincide. Note that while this is not strictly speaking a plasma ($a \approx \lambda_d$), the equilibrium equation still applies.[5]

2. Parabolic temperature profile

To demonstrate the effect of nonuniform temperature, a parabolic temperature distribution is applied such that $\alpha(\psi)$ [Eq. (2)] goes from 1 at the magnetic axis to 0.01 at the outer magnetic surface. A plasma with a few Debye lengths is chosen such that both potential and density vary on magnetic surfaces.

The top plot of Fig. 3 shows contours for the constant temperature case, while the lower plot represents a parabolic temperature profile. The two plots are virtually identical near the magnetic axis, where the temperatures are similar. It is only near the edge of the plasma that the parabolic case differs, in that the potential varies less on a magnetic surface and the density varies more. This behavior is exactly what one would expect based on the results of the preceding section, since in the parabolic case the plasma is colder (has a shorter Debye length) near the edge.

3. Vertically shifted surfaces

For the following equilibria, the magnetic surfaces are shifted downward with respect to the conducting boundary. This demonstrates the effect of a conducting boundary that does not match the outer magnetic surface of a plasma.

A plasma with many Debye lengths ($a \approx 10\lambda_d$) is shown in Fig. 4 (top). The outer magnetic contour represents the boundary of the plasma, while the outer potential contour is the conducting boundary. The potential is nearly constant on the magnetic surfaces in the interior of the plasma, but deviates near the plasma edge.

The plasma itself is shifted towards the near wall of the conductor, decreasing the energy associated with the interac-

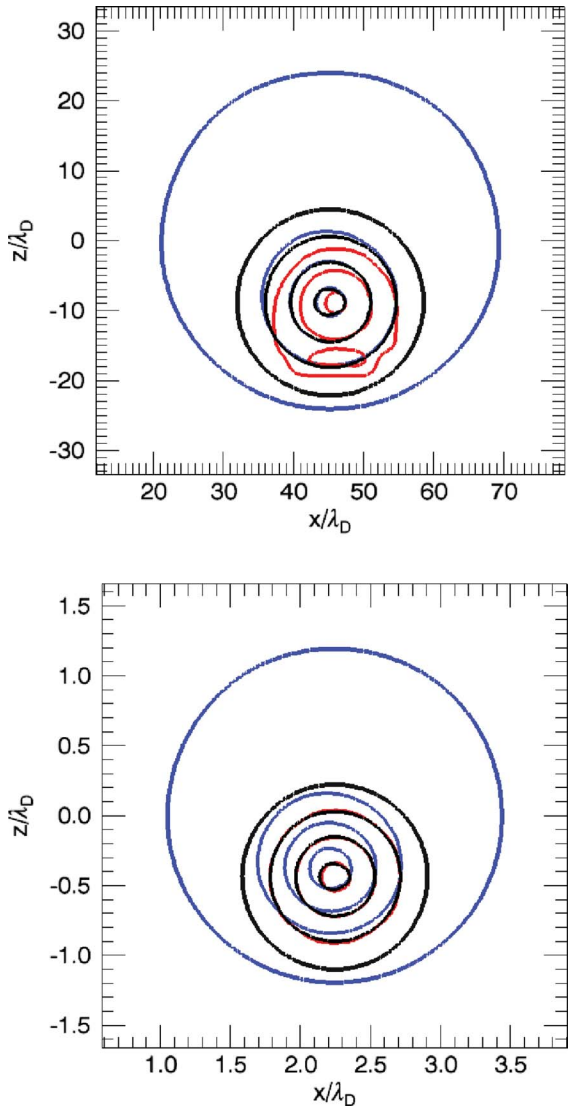

FIG. 4. (Color). Shifted magnetic surfaces. Many Debye lengths (top), few Debye lengths (bottom). Contours of constant Φ (blue), n (red), and ψ (black) for a plasma with nonconforming equipotential boundary.

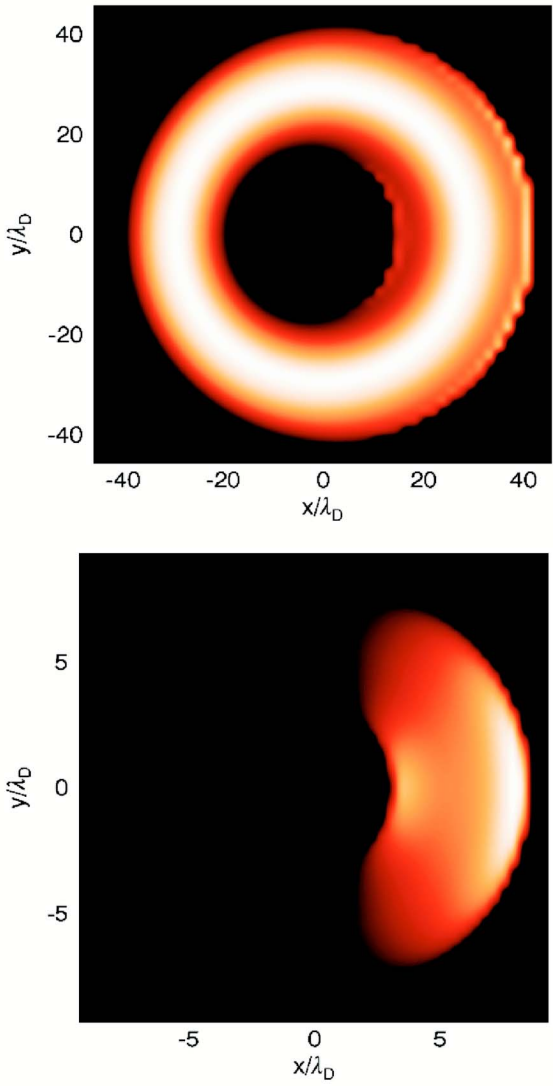

FIG. 5. (Color online). Biased boundary. Dense/large (top), rare/small (bottom). Plasma density (lighter=denser) at a cut through the x-y plane, at $z=0$, for a plasma with boundary biased as $\cos(\phi)$.

tion between the plasma and the image charge. This is what one would expect from a stable equilibrium, but the opposite of what occurs in a Penning trap, which has a maximum energy equilibrium state. It has recently been shown that the equilibrium is a minimum energy state with respect to slow perturbations.[12]

A plasma with fewer Debye lengths ($a \approx \lambda_d$) is shown in Fig. 4 (bottom). The pressure dominates in this case, spreading the plasma evenly over each magnetic surface. There are not enough Debye lengths in this plasma for effective Debye screening. Again, since there is no conductor on the outer magnetic surface of the plasma, the potential contours deviate most near the edge of the plasma where the density is lowest and the local Debye length is longest.

4. Conforming, biased boundary

By imposing some potential on the boundary that is a function of the coordinate ϕ, we can explore the effect of biasing segmented conductors. In the following we present equilibria for the case where the potential on the boundary is given by $\tilde{\Phi}_b = A\cos(\phi)$, with a dimensionless amplitude $A=5$. This is achieved using the SVD method in the same manner as for an equipotential conducting boundary.

A density profile through the x-y plane is shown in Fig. 5 (top) for a plasma with ($a \approx 10\lambda_d$). Lighter regions of the plot represent higher densities. The central density is nearly constant in ϕ, while Debye shielding effects can be seen near the edges. There is a buildup of charge near the plasma edge on the high-potential (right) side of the torus (for an electron plasma), and a depletion on the low-potential side (left).

A plasma containing fewer Debye lengths ($a \approx \lambda_d$) is shown in Fig. 5 (bottom). Recall that the magnitude of the potential on the boundary is $\tilde{\Phi} = e\Phi/T_e = 5$. We can think of this plasma as being less dense or smaller than the previous one, while having the same temperature so that the magnitude of the applied (dimensional) potential remains the same. A hollow density profile results around $\phi=0$ due to the

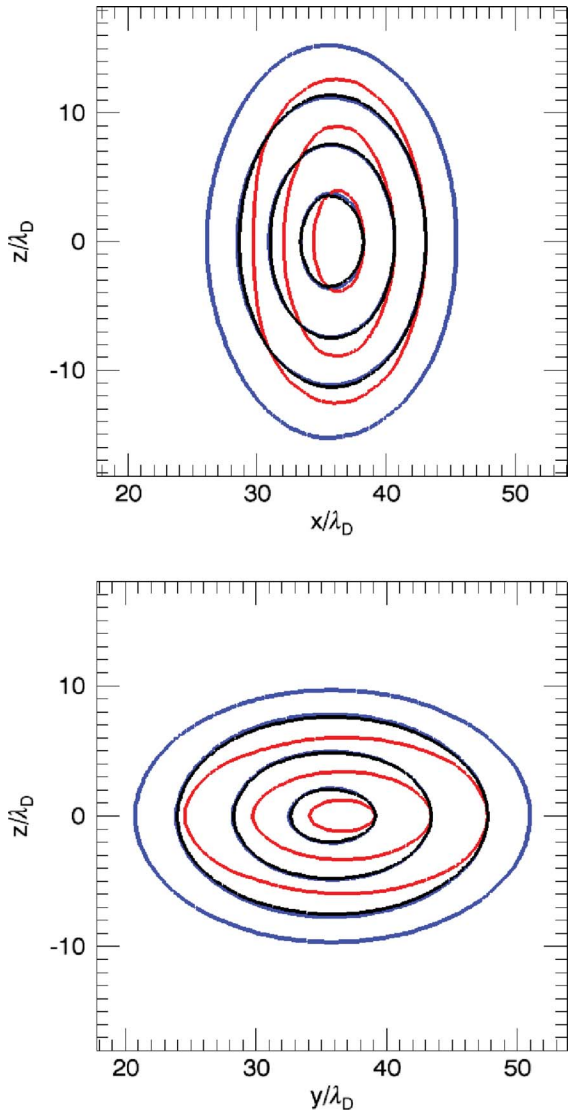

FIG. 6. (Color). Helically symmetric surfaces. $\phi=0$ (top), $\phi=\pi/2$ (bottom). Contours of constant Φ (blue), n (red), and ψ (black) for an $a/\lambda_D \approx 10$ plasma.

strong attraction of the plasma to the biased conductor. In this case, Debye shielding is ineffective due to the low density or small size of the plasma, and the low-potential side of the torus is completely evacuated.

B. Toroidally asymmetric surfaces

1. Helically symmetric surfaces

The computational method developed to solve the equilibrium equation is capable of handling a variety of magnetic surface and boundary shapes. In this section we present results for a typical stellarator type configuration, with helically symmetric magnetic surfaces and conforming equipotential boundary (as in Fig. 1). The magnetic surfaces and equipotential boundary are created by sweeping an elliptical cross section through ϕ, rotating the section once in θ during the revolution.

Contours are shown for toroidal cross sections at $\phi=0$ and $\phi=\pi/2$ in Fig. 6. This is a plasma with many Debye lengths ($a \approx 10\lambda_d$), so Φ contours are barely distinguishable from ψ contours. The same outward shift of density is observed as in the toroidally symmetric case. There is also an increase in the ellipticity of the density contours, regardless of the orientation of the elliptical ψ contours. This agrees with the results seen previously in 2D calculations,[8] and is therefore an effect of ellipticity rather than toroidicity. On each surface, the density is highest at the two far ends of the ellipse. This reduces the interaction energy of the electrons as compared to an even spread over the elliptical cross section.

FIG. 7. (Color online). Cutaway view of the CNT magnetic surface configuration.

2. CNT equilibria

The Columbia Non-Neutral Torus has a twice-periodic, fully three-dimensional magnetic surface configuration in which the cross section varies significantly over a toroidal quarter period (Fig. 7). It is the lowest aspect ratio stellarator ever built ($1/\epsilon \approx 1.8$), as recently confirmed by field-line mapping experiments. Diagnostics and electron emitters are currently being tested, and a conducting boundary is being constructed, in preparation for first plasma.

Equilibria for a plasma with $a/\lambda_D \approx 1$ are shown in Fig. 8 for two toroidal locations, the most elongated cross section at $\phi=0$ and the roundest cross section at $\phi=\pi/2$. As with previous equilibria, the density is roughly constant on each magnetic surface and the potential varies significantly when there are few Debye lengths in the plasma. Note that the potential contours that appear outside of the equipotential boundary are merely artifacts of the complicated image charge distribution required for this configuration.

A plasma with $a/\lambda_D \approx 10$ is shown in Fig. 9. Both cross sections demonstrate the near constancy of the potential on a magnetic surface that was observed with simpler configurations, as well as the increase in ellipticity and outward shift of the density contours.

The $\phi=\pi/2$ contour exhibits a peaking of the density above and below the magnetic axis, a saddle-type distribution that was not present in the previously presented equilibria. This broad qualitative effect should be easy to diagnose in the CNT, if present. Note that this is the cross section at

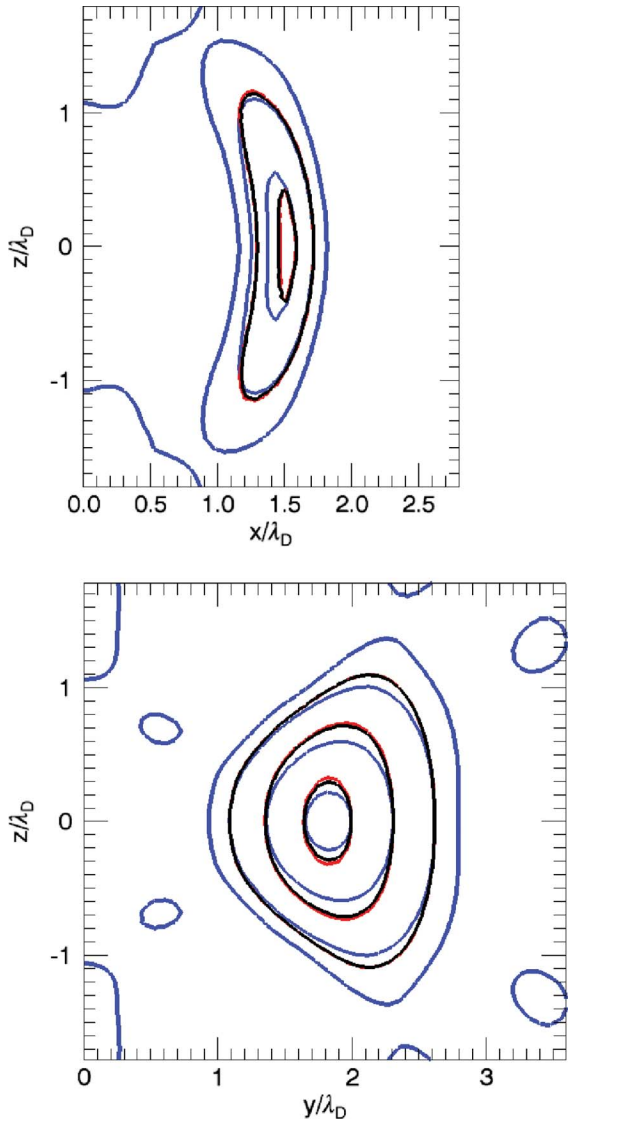

FIG. 8. (Color). CNT Equilibria, $a/\lambda_D \approx 1$. $\phi=0$ (top), $\phi=\pi/2$ (bottom). Contours of constant Φ (blue), n (red), and ψ (black).

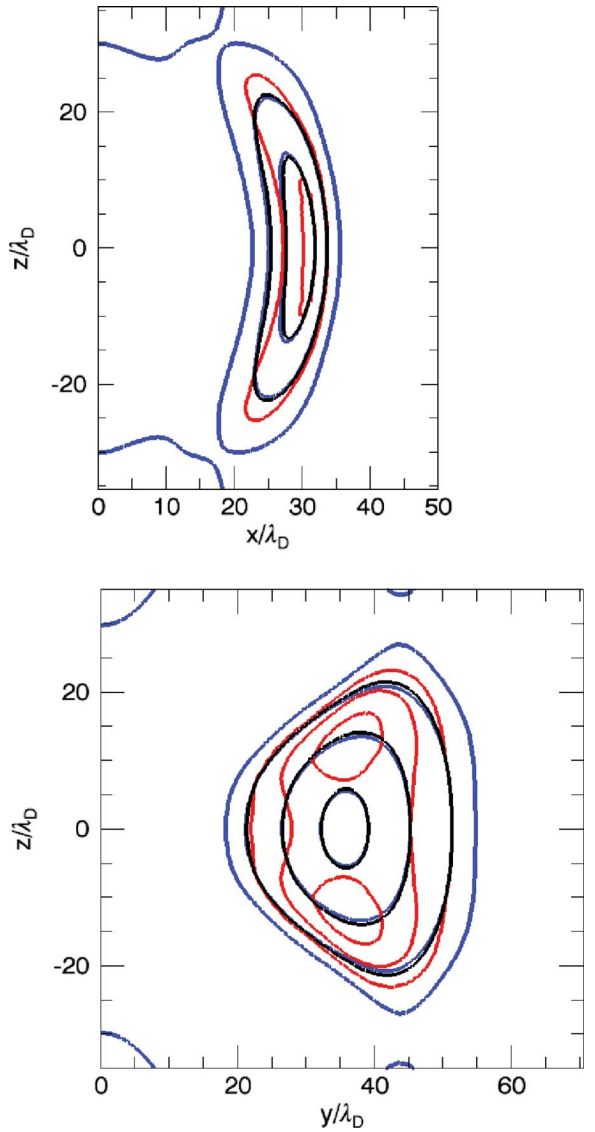

FIG. 9. (Color). CNT equilibria, $a/\lambda_D \approx 10$. $\phi=0$ (top), $\phi=\pi/2$ (bottom). Contours of constant Φ (blue), n (red), and ψ (black).

which the line of parabolic density is imposed, at $z=0$, from the magnetic axis to the outboard side of the outer magnetic surface.

V. DISCUSSION

Using a simple numerical technique, equilibrium profiles of single species plasmas confined on magnetic surfaces have been determined for a wide range of boundary conditions and magnetic surface configurations. The equilibrium equation represents a parallel balance between the electrostatic force and the pressure gradient combined with Poisson's equation for the electrostatic potential. The only parameter that distinguishes one equilibrium from another is the number of Debye lengths in the plasma: we can think of $a \gg \lambda_D$ plasmas as large/cold/dense and $a \ll \lambda_D$ "plasmas" as small/hot/rare.

Like the Shafranov shift of quasineutral plasmas, single-species plasmas confined on magnetic surfaces are shifted outward. However, the magnetic surfaces in the single-species case are rigid and the outward shift of the plasma is a result of the electrostatic hoop force pushing the plasma to the outboard side of the magnetic surfaces. This is the opposite of what occurs in non-neutral plasmas confined by pure toroidal fields which shift inward, such that the resulting attraction of the plasma to the inboard side of the conducting boundary balances the hoop force.[9–11]

When the conducting boundary is shifted vertically with respect to the magnetic surfaces, the plasma density builds up near the conductor. This is equivalent to a negatively charged plasma being attracted to a positive charge. It is consistent with a minimum energy state,[12] which we expect from a stable system, but the opposite of what occurs in pure toroidal field confinement of single-species plasmas.

Single-species plasmas exhibit Debye screening in a manner similar to quasineutral plasmas. For instance, where there would be a buildup of positive charge density around a negative test charge in a quasineutral plasma, there is a depletion of density in a pure electron plasma. This is dem-

onstrated by the equilibrium profiles of plasmas with nonuniformly biased boundaries, and plasmas with nonconforming equipotential boundaries. Because of this depletion effect, entire regions can become fully evacuated, rendering the shielding mechanism ineffective.

The Φ contours closely follow the ψ contours for plasmas containing a significant number of Debye lengths ($a \gtrsim 10\lambda_D$). This means that the $\mathbf{E}\times\mathbf{B}$ drift is within a surface, so cross-surface transport is lower and confinement better for denser plasmas, providing $n \ll n_B = \epsilon_0 B^2/2m_e$ and $n \ll \epsilon_0 Bc/ae$ are satisfied. The worst confinement tends to occur near the edge of the plasma, where the density is lowest, the local Debye length is longest, and the alignment of Φ and ψ contours is poorest. This suggests that the density profile will become narrower and steeper through shedding of the outer layers, although the dynamics of this have not been studied. A conducting boundary that matches a magnetic surface on the edge of the plasma helps confinement by forcing the potential and magnetic contours to coincide in this region. The implementation of such a conducting boundary is simple for low-density non-neutral plasmas confined in a stellarator configuration, since plasma currents do not modify the magnetic surfaces.

The computed CNT equilibria exhibit the same near-constancy of electric potential on a magnetic surface that is exhibited by simpler geometries with the same number of Debye lengths, $a \approx 10\lambda_D$. This is promising in terms of expected confinement time, provided a sufficiently cold and dense plasma can be initiated.

ACKNOWLEDGMENT

This material is based upon the work supported by the National Science Foundation under Grant No. 0317359.

[1] T. S. Pedersen, A. H. Boozer, J. P. Kremer, R. Lefrancois, F. Dahlgren, N. Pomphrey, W. Reiersen, and W. Dorland, Fusion Sci. Technol. **46**, 200 (2004).
[2] T. S. Pedersen, A. H. Boozer, J. P. Kremer, and R. Lefrancois, Phys. Plasmas **11**, 2377 (2004).
[3] T. S. Pedersen, A. H. Boozer, W. Dorland, J. P. Kremer, and R. Schmitt, J. Phys. B **36**, 1029 (2003).
[4] L. Brillouin, Phys. Rev. **67**, 260 (1945).
[5] T. S. Pedersen and A. H. Boozer, Phys. Rev. Lett. **88**, 205002 (2002).
[6] E. M. Hollmann, F. Anderegg, and C. F. Driscoll, Phys. Plasmas **7**, 1767 (2000).
[7] T. O'Neil and R. Smith, Phys. Plasmas **1**, 2430 (1994).
[8] T. S. Pedersen, Phys. Plasmas **10**, 334 (2003).
[9] K. Avinash, Phys. Fluids B **3**, 3226 (1991).
[10] P. Zaveri, P. John, K. Avinash, and P. Kaw, Phys. Rev. Lett. **68**, 3295 (1992).
[11] J. Daugherty and R. Levy, Phys. Fluids **10**, 155 (1967).
[12] A. H. Boozer, Phys. Plasmas **11**, 4709 (2004).